Optimal rotary control of the cylinder wake in the laminar regime

B. Protas[a)]
Department of Aerodynamics, Institute of Aeronautics and Applied Mechanics, Warsaw University of Technology, ul. Nowowiejska 24, 00-665 Warsaw, Poland and Laboratoire de Physique et Mécanique des Milieux Hétérogènes, École Supérieure de Physique et Chimie Industrielles, 10 rue Vauquelin, 75231 Paris Cedex 05, France

A. Styczek
Department of Aerodynamics, Institute of Aeronautics and Applied Mechanics, Warsaw University of Technology, ul. Nowowiejska 24, 00-665 Warsaw, Poland

(Received 17 November 2000; accepted 18 March 2002; published 20 May 2002)

In this paper we develop the Optimal Control Approach to the rotary control of the cylinder wake. We minimize the functional which represents the sum of the work needed to resist the drag force and the work needed to control the flow, where the rotation rate $\dot{\varphi}(t)$ is the control variable. Sensitivity of the functional to control is determined using the adjoint equations. We solve them in the ''vorticity'' form, which is a novel approach and leads to computational advantages. Simulations performed at $Re=75$ and $Re=150$ reveal systematic decrease of the total power and drag achieved using a very small amount of control effort. We investigate the effect of the optimization horizon on the performance of the algorithm and the correlation of the optimal controls with the changes of the flow pattern. The algorithm was also applied to the control of the subcritical flow at $Re=40$, however, no drag reduction was achieved in this case. Based on this, limits of the performance of the algorithm are discussed. © *2002 American Institute of Physics.* [DOI: 10.1063/1.1476671]

I. INTRODUCTION

The general objective of flow control is to design a small [on the order of $O(\epsilon)$] input to the system, i.e., the *control*, that will result in a significant [on the order of $O(1)$] output with desired properties. Given the nonlinear character of the governing equations and the chaotic nature of their solutions, the problem of controlling the fluid flow is highly nontrivial and does not admit general and uniformly valid solutions. Many different approaches have been proposed and have achieved varying degrees of success. In the present investigation we are interested in the fundamental problem of controlling the nonstationary wake behind the circular cylinder. This flow configuration is regarded as a prototype of separated flows and at the same time is sufficiently simple to admit numerical solution at a reasonable cost. It is, therefore, a convenient testbed for developing algorithms which can be later applied to more complex configurations. The flow domain Ω is assumed to be infinite. The oncoming flow is uniform at infinity and has velocity $\boldsymbol{V}_\infty$ (see Fig. 1). Wake flows are characterized by the Reynolds number defined as $Re=|\boldsymbol{V}_\infty|D/v$, where v is the kinematic viscosity of the fluid and D is the cylinder diameter. Control is applied in the form of the rotary motion of the obstacle and is characterized by the instantaneous rotation rate $\dot{\varphi}(t)$. It is equivalent to specifying the tangential boundary velocity $V_\tau(t)$. By controlling the flow we seek to reduce the drag, i.e., the horizontal component of the force, using the smallest possible control effort. Most theoretical considerations discussed in this study are not restricted by the Reynolds number. However, all computational investigations presented here will concern the two-dimensional laminar regime. Given the well-known limitations of the 2D model for the description of the wake flow (e.g., Refs. 1 and 2), our simulations are restricted to the plane case with $Re=75$ and $Re=150$. For $Re\leqslant 180$ cylinder wake flows are known to remain two-dimensional (2D) (see, e.g., Williamson in Ref. 3). This allows us to use 2D simulations in this regime. Additional simulations are also performed for the subcritical case with $Re=40$.

From the physical point of view, our primary motivation comes from the laboratory experiments by Tokumaru and Dimotakis.[4] They showed that by using a very simple harmonic rotation of the obstacle one can obtain significant drag reduction reaching 80% at $Re=15\,000$. This effect was further investigated by Shields in Ref. 5 and Lu and Sato in Ref. 6. In recent investigations He *et al.*[7] and Homescu *et al.*[8] applied the tools of the Optimal Control Theory to optimize the harmonic control of the wake. In a related study (Ref. 9) we however obtained evidence showing that for $Re=150$ the harmonic rotary control is energetically inefficient, i.e., the control power far exceeds the gain in the drag power. In the present investigation we seek to optimize the rotary motion of the obstacle so as to make the control more efficient from the point of view of energy budget. We are interested in assessing the inherent capabilities and limitations of such an approach. In the context of feedback wake control, most of similar investigations dealt with the blowing-and-suction control, e.g., Gunzburger and Lee in Ref. 10 and Park in Ref.

[a)]Author to whom correspondence should be addressed. Present address: Department of MAE, UCSD, 9500 Gilman Dr., La Jolla, CA 92093-0411. Telephone: (858) 822-3391; fax: (858) 822-3107; electronic mail: bprotas@ucsd.edu

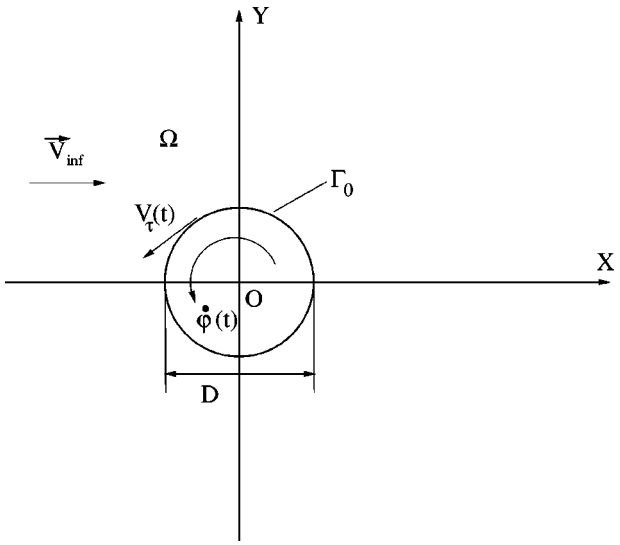

FIG. 1. Flow configuration with control.

11, or acoustic actuation, e.g., Roussopoulos in Ref. 12. In all of these works the authors relied on intuition to identify the critical physical mechanisms which were then controlled. An alternative approach consists in extracting a low-dimensional approximation of the system, the so-called Reduced Order Model, which is subjected to control. In the context of wake flows these concepts were developed in the works by Graham *et al.*,[13,14] Chernyshenko,[15] Cortelezzi,[16] and Cortelezzi *et al.*[17]

For the theoretical part, the present investigation builds on the study by Abergel and Temam[18] which was the first formulation of a flow control problem in terms of the modern Optimal Control Theory, an extension of the seminal work by Lions.[19] This approach was first applied in the suboptimal setting, i.e., with the vanishing optimization horizon, to the control of the stochastic Burgers equation by Choi *et al.* in Ref. 20 and then to the control of the turbulent channel flow by Lee *et al.* in Ref. 21. The finite horizon optimal control of the channel flow was then systematically investigated by Bewley *et al.* in Ref. 22. As regards the wake flow, an optimal control approach was considered theoretically by Sritharan in Ref. 23 and computationally by Min and Choi[24] (the latter study, however, concerns the blowing-and-suction type of control in the suboptimal setting). Therefore, the main objective of the present study is to develop an optimal control approach for drag minimization in the cylinder wake in the case when the rotary motion of the obstacle is the control. Furthermore, the formalism is extended and recast in terms of the nonprimitive variables, i.e., velocity–vorticity, instead of velocity–pressure.

The flow of viscous incompressible fluid is governed by the Navier–Stokes system

$$\begin{aligned}
&\frac{\partial \boldsymbol{V}}{\partial t}+(\boldsymbol{V}\cdot\nabla)\boldsymbol{V}=-\nabla p+\mu\Delta\boldsymbol{V},\\
&\nabla\cdot\boldsymbol{V}=0,\\
&\boldsymbol{V}|_{t=0}=\boldsymbol{V}_0 \quad \text{in} \quad \Omega,\\
&\boldsymbol{V}=\boldsymbol{b}(\dot{\varphi}) \quad \text{on} \quad \Gamma_0, \quad \boldsymbol{V}\to\boldsymbol{V}_\infty \quad \text{for} \quad |x|\to\infty,
\end{aligned} \tag{1}$$

where $\boldsymbol{V}$ is the velocity field, p is pressure, and μ is the coefficient of viscosity. The system is supplemented with the boundary conditions $\boldsymbol{b}(\dot{\varphi})$ representing the motion of the boundary as a function of the rotation rate $\dot{\varphi}$, $\boldsymbol{V}_\infty$ representing the free stream at infinity, and the initial condition $\boldsymbol{V}_0$. In all the simulations reported here the initial condition $\boldsymbol{V}_0$ will correspond to the developed wake flow with saturated vortex shedding. When one is studying external flows, it is often more convenient to use the vorticity (i.e., the nonprimitive) form of the system (1). It is obtained by taking the curl of the Navier–Stokes system and in 2D (i.e., when $\boldsymbol{V}=[u,v,0]$) is expressed as

$$\begin{aligned}
&\frac{\partial\omega}{\partial t}+(\boldsymbol{V}\cdot\nabla)\omega=\mu\Delta\omega,\\
&\omega=\frac{\partial v}{\partial x}-\frac{\partial u}{\partial y}, \qquad \frac{\partial u}{\partial x}+\frac{\partial v}{\partial y}=0,\\
&\boldsymbol{V}|_{t=0}=\boldsymbol{V}_0 \quad \text{in} \quad \Omega,\\
&\boldsymbol{V}=\boldsymbol{b}(\dot{\varphi}) \quad \text{on} \quad \Gamma_0, \quad \boldsymbol{V}\to\boldsymbol{V}_\infty \quad \text{for} \quad |x|\to\infty,
\end{aligned} \tag{2}$$

where ω denotes vorticity. In the case of multiconnected flow domains this system must be supplemented by the following constraint on the vorticity production on the boundary of every ''hole'' in the flow domain (for derivation see, for example, the study by Gunzburger and Peterson[25])

$$\mu\int_0^L\frac{\partial\omega}{\partial n}d\sigma=\int_0^L\left[\frac{\partial\boldsymbol{V}}{\partial t}\cdot\boldsymbol{\tau}+(\boldsymbol{V}\cdot\boldsymbol{n})\omega\right]d\sigma, \tag{3}$$

where the integrals are taken along the contour perimeter $[0;L]$. This constraint ensures that the field $\boldsymbol{V}-\boldsymbol{V}_\infty$ has finite kinetic energy and that pressure, when recovered *a posteriori* from the velocity and vorticity fields, is single valued. The advantage of using formulations (2) and (3) is that it is based on a more localized variable (vorticity). Its support is quasicompact, as opposed to velocity and pressure. This is particularly convenient when one is studying flows in infinite domains.

The paper is organized as follows: in the next two sections we outline the Optimal Control Algorithm and derive the ''vorticity'' form of the adjoint equations, then we briefly describe the Vortex Method which is used here to solve the hydrodynamic equations and also the adjoint system; in Sec. V we present and discuss the results of the computations; final conclusions come in Sec. VI. In the Appendix we present some technical details concerning the derivation of the adjoint system.

II. OPTIMAL CONTROL ALGORITHM

The starting point is the formulation of the specific functional that will be minimized. In our case it represents the balance over the time interval $[0;T]$ of the work that has to be done against the drag force and the work needed to control the flow

$$J(\dot{\varphi}) = \frac{1}{2}\int_0^T \left\{ \begin{bmatrix} \text{power related to} \\ \text{the drag force} \end{bmatrix} + \begin{bmatrix} \text{power needed to} \\ \text{control the flow} \end{bmatrix} \right\} dt. \tag{4}$$

The rotation rate $\dot{\varphi}(t)$ of the cylinder is the control (Fig. 1), therefore, the energy needed to control the flow is introduced in the form of the moment of forces, the torque, applied to the cylinder. Here we do not take into account the moment of inertia of the cylinder, as it is entirely material-dependent and therefore can be arbitrary. Consequently, using the surface force density $\boldsymbol{f}(\dot{\varphi})$, the above relation can be expressed as

$$\begin{aligned} J(\dot{\varphi}) &= \frac{1}{2}\int_0^T \oint_{\Gamma_0} \{\boldsymbol{f}(\dot{\varphi})\cdot\boldsymbol{V}_\infty + [\boldsymbol{r}\times\boldsymbol{f}(\dot{\varphi})]\cdot(\dot{\varphi}\boldsymbol{e}_z)\} d\sigma dt \\ &= \frac{1}{2}\int_0^T \oint_{\Gamma_0} \{\boldsymbol{f}(\dot{\varphi})\cdot[\dot{\varphi}(\boldsymbol{e}_z\times\boldsymbol{r}) + \boldsymbol{V}_\infty]\} d\sigma dt \\ &= \frac{1}{2}\int_0^T \oint_{\Gamma_0} \{[p(\dot{\varphi})\boldsymbol{n} - \mu\boldsymbol{n}\cdot\bar{\bar{D}}(\boldsymbol{V}(\dot{\varphi}))] \\ &\quad \cdot[\dot{\varphi}(\boldsymbol{e}_z\times\boldsymbol{r}) + \boldsymbol{V}_\infty]\} d\sigma dt, \end{aligned} \tag{5}$$

where all the hydrodynamic quantities depend on the control $\dot{\varphi}$. Here $\bar{\bar{D}}(\boldsymbol{V}) = [\nabla\boldsymbol{V} + (\nabla\boldsymbol{V})^T]$ is the rate-of-strain tensor of the field $\boldsymbol{V}$ and $\boldsymbol{e}_z$ the versor of the z axis (normal to the flow plane).

The optimal control $\dot{\varphi}_{\text{opt}}$ and the related optimal state $\{\boldsymbol{V}(\dot{\varphi}_{\text{opt}}); p(\dot{\varphi}_{\text{opt}})\}$ correspond to the minimum of the functional (5) and are therefore characterized by the vanishing of its Gâteaux differential

$$J'(\dot{\varphi}_{\text{opt}}; h) = 0, \tag{6}$$

where h represents an arbitrary direction in the space of controls in which the differential is computed. We note that (6) is only a necessary, but not sufficient, condition for optimality and, since the governing equation (1) is nonlinear, convexity of the functional (5) cannot be ensured and the optimum is only local. The Gâteaux differential represents the linear part of the functional increment that results from applying the perturbation h to control and evaluated in the neighborhood of the state $\{\boldsymbol{V}_0(\dot{\varphi}); p_0(\dot{\varphi})\}$. For the case of the functional (5), the Gâteaux differential takes the form

$$\begin{aligned} J'(\dot{\varphi}; h) = \frac{1}{2}\int_0^T \oint_{\Gamma_0} &\{[q(h)\boldsymbol{n} - \mu\boldsymbol{n}\cdot\bar{\bar{D}}(\boldsymbol{w}(h))] \\ &\cdot[\dot{\varphi}(\boldsymbol{e}_z\times\boldsymbol{r}) + \boldsymbol{V}_\infty] + [p_0(\dot{\varphi})\boldsymbol{n} - \mu\boldsymbol{n} \\ &\cdot\bar{\bar{D}}(\boldsymbol{V}_0(\dot{\varphi}))]\cdot(\boldsymbol{e}_z\times\boldsymbol{r})h\} d\sigma dt, \end{aligned} \tag{7}$$

where the quantities $\{\boldsymbol{w}(h); q(h)\}$ are the solution of the Navier–Stokes system (1) linearized about the state $\{\boldsymbol{V}_0; p_0\}$ (see the Appendix for details). It should be observed that for the circular cylinder the vectors $\boldsymbol{n}$ and $\boldsymbol{r}$ are collinear, hence $\boldsymbol{n}\cdot(\boldsymbol{e}_z\times\boldsymbol{r}) = 0$ and the pressure term in (7) drops out. The Gâteaux differential will now be used to extract the functional gradient ∇J according to $J'(\dot{\varphi}; h) = (\nabla J, h)_{L_2([0,T])}$. However, the expression (7) does not have a form convenient for this purpose, as the control perturbation h enters implicitly through the solution of the linearized problem. The now classical approach (see Lions,[19] Abergel and Temam,[18] and Bewley *et al.*[26]) consists in using the adjoint operator N^* and the associated adjoint state $\{\boldsymbol{w}^*; q^*\}$ to reexpress (7) so that the control perturbation h appears as a factor. This yields

$$\begin{aligned} J'(\dot{\varphi}; h) &= \int_0^T \nabla J(t) h dt \\ &= \frac{1}{2}\int_0^T \oint_{\Gamma_0} \{\mu R\boldsymbol{n}\cdot\bar{\bar{D}}(\boldsymbol{w}^*)\cdot\boldsymbol{\tau} \\ &\quad + \mu\boldsymbol{n}\cdot\bar{\bar{D}}(\boldsymbol{V}_0(\dot{\varphi}))\cdot(\boldsymbol{e}_z\times\boldsymbol{r})\} h d\sigma dt, \end{aligned} \tag{8}$$

where R is the cylinder radius and $\boldsymbol{\tau}$ the unit tangent vector, whereas $\boldsymbol{w}^*$ is a solution of the system adjoint to the Navier–Stokes equations linearized about the state $\{\boldsymbol{V}_0; p_0\}$. The adjoint system has the form

$$\begin{aligned} &N^*\begin{bmatrix} \boldsymbol{w}^* \\ q^* \end{bmatrix} = \begin{bmatrix} -\dfrac{\partial\boldsymbol{w}^*}{\partial t} - \boldsymbol{V}_0\cdot[\nabla\boldsymbol{w}^* + (\nabla\boldsymbol{w}^*)^T] - \mu\Delta\boldsymbol{w}^* + \nabla q^* \\ -\nabla\cdot\boldsymbol{w}^* \end{bmatrix} = \begin{bmatrix} 0 \\ 0 \end{bmatrix}, \\ &\boldsymbol{w}^*|_{t=T} = 0 \quad \text{in } \Omega, \\ &\boldsymbol{w}^* = \boldsymbol{r}\times(\dot{\varphi}\boldsymbol{e}_z) + \boldsymbol{V}_\infty \quad \text{on } \Gamma_0, \quad \boldsymbol{w}^* \to 0 \quad \text{for } |x| \to \infty. \end{aligned} \tag{9}$$

For complete derivation we refer the reader to the Appendix. The functional setting and issues related to the existence of solutions for a very similar problem were addressed in detail by Fursikov *et al.* in Ref. 27. Here we note that (9) is in fact a *terminal value problem*, i.e., it has to be marched backward in time. The system is nevertheless well-posed, as using the substitution $t = T - \tau$ we arrive at a problem similar to the advection-diffusion equation (this substitution, however, reverses the field $\boldsymbol{V}_0$ in which advection takes place). The adjoint system (9) involves the primal field $\boldsymbol{V}_0$ as coefficients and is forced through the boundary conditions corresponding to the quantities measured by the functional (5). Applying the identity $J'(\dot{\varphi}; h) = (\nabla J, h)_{L_2([0,T])}$ to (8) we can now extract the functional gradient as

$$\nabla J(t) = \tfrac{1}{2}\mu R \oint_{\Gamma_0} \boldsymbol{n} \cdot [\bar{\bar{D}}(\boldsymbol{w}^*) + \bar{\bar{D}}(\boldsymbol{V}_0(\dot{\varphi}_{\mathrm{opt}}))] \cdot \boldsymbol{\tau} d\sigma = \tfrac{1}{2}\mu R^2 \int_0^{2\pi} [(s_{11}^0 + s_{11}^*)(-\sin(2\theta)) + (s_{12}^0 + s_{12}^*)\cos(2\theta)] d\theta, \tag{10}$$

where s_{11}^0, s_{12}^0, s_{11}^*, and s_{12}^* are the components of the rate-of-strain tensor for the primal and the adjoint field, $\bar{\bar{D}}(\boldsymbol{V}_0)$ and $\bar{\bar{D}}(\boldsymbol{w}^*)$, respectively. Thus $-\nabla J(t)$ represents the direction in which the control corresponding to the state $\{\boldsymbol{V}_0(\dot{\varphi}); p_0(\dot{\varphi})\}$ should be updated in order to decrease the functional (5). Upon multiplying the gradient $\nabla J(t)$ by some $h(t)$ and integrating over $[0;T]$, we obtain the first-order approximation to the change of the functional due to the perturbation h. Therefore, the adjoint state $\{\boldsymbol{w}^*; q^*\}$ admits a clear physical interpretation—the adjoint strain on the boundary carries information about the sensitivity of the functional (5) to the given type of forcing. Evidently, apart from the adjoint fields, to compute $\nabla J(t)$ we also need the primal state $\{\boldsymbol{V}_0(\dot{\varphi}); p_0(\dot{\varphi})\}$ at which the gradient is evaluated. We remark that the above derivation is fairly general and so far we have not introduced any assumptions restricting the flow to two dimensions.

Now an iterative gradient procedure will be presented which can be used to find the optimal control $\dot{\varphi}_{\mathrm{opt}}$ and the corresponding optimal state $\{\boldsymbol{V}(\dot{\varphi}_{\mathrm{opt}}); p(\dot{\varphi}_{\mathrm{opt}})\}$ in the time interval $[0;T]$. First, we choose some initial guess $\dot{\varphi}^1$ for control (for instance $\dot{\varphi}^1 \equiv 0$) and then sequentially compute the functional gradient $\nabla J(t)$ and update the time-dependent control accordingly. This involves the following steps (here the superscripts i denote the consecutive iterations):

(1) solve the full nonlinear Navier–Stokes system in order to determine $\{\boldsymbol{V}_0(\dot{\varphi}^i); p_0(\dot{\varphi}^i)\}$ around which linearization is made;
(2) solve (9) for the adjoint state $\{\boldsymbol{w}^{*i}; q^{*i}\}$ (in the neighborhood of $\{\boldsymbol{V}_0(\dot{\varphi}^i); p_0(\dot{\varphi}^i)\}$);
(3) use $\{\boldsymbol{V}_0(\dot{\varphi}^i); p_0(\dot{\varphi}^i)\}$ and $\{\boldsymbol{w}^{*i}; q^{*i}\}$ to determine the functional gradient $\nabla J^i(t)$ on the interval $[0;T]$;
(4) use $\nabla J^i(t)$ to update the control according to $\dot{\varphi}^{i+1}(t) = \dot{\varphi}^i(t) - \alpha_i \gamma_i(\nabla J(t))$, where α_i is some properly tuned descent parameter and γ_i is the descent direction;
(5) iterate (1)–(4) until convergence, i.e., until $\nabla J^i(t) = 0$ attains in some approximate sense.

Now it must be explained how the gradient information ∇J^i is used to determine the descent direction γ_i. Guided by Bewley *et al.*,[22] we use the Polak–Ribiere version of the Conjugate Gradient Algorithm (see Polak[28]). In every iteration the control is updated according to

$$\dot{\varphi}^{i+1} = \dot{\varphi}^i - \alpha_i \gamma_i, \tag{11}$$

where γ_i represents the conjugate direction given by

$$\gamma_i = \nabla J^i - \beta_i \gamma_{i-1}, \quad \gamma_1 = \nabla J^1, \tag{12}$$

with β_i standing for the ''momentum'' parameter

$$\beta_i = \frac{((\nabla J^i - \nabla J^{i-1}), \nabla J^i)}{(\nabla J^{i-1}, \nabla J^{i-1})}. \tag{13}$$

We remind that $\dot{\varphi}^{i+1}$, $\dot{\varphi}^i$, and γ_i are all functions of time, but the corresponding notation is suppressed here for brevity. The value of the parameter α_i is adjusted in the course of a line minimization procedure which minimizes the functional along the descent direction. For this we use the Brent's method (see Press *et al.*[29]) combining the golden section search with parabolic interpolation. Such an approach ensures robustness in the initial bracketing of the minimum, performed as the golden section search, with fast convergence when parabolic interpolation takes over. As will become apparent later on, line minimization involves a trade-off between accuracy and the number of flow evaluations (they account for the major part of the overall computational cost). For nearly quadratic functionals the Conjugate Gradient Method is known to assure fastest convergence, much better than the simple steepest descent method. Iterations are terminated when in a given number of functional evaluations (usually 4 to 5) the updated control does not decrease the functional. This may also happen when the initial guess for α_i falls outside the validity range of the linear approximation to the functional increment given by the Gâteaux differential. In principle, the extent of this range is not known *a priori* and may be different for problems on different optimization intervals. Consequently, in order to ensure rapid convergence of line minimization in all the investigated configurations, the initial guess for α_i is adjusted by trial and error. We emphasize that this is done to enhance performance without compromising accuracy and in principle, when the number of available flow evaluations is large, the optimal α_i can be found starting from any sufficiently small initial guess.

The procedure described above allows us to minimize the functional over the optimization interval T. Ideally, one would wish to extend T so as to cover the whole time-span over which flow control is attempted. This would, however, result in an intractable computational task. Even more importantly, as reported by Bewley *et al.*,[22] the problem may for long T become strongly nonconvex and have many local minima. Consequently, optimization must be independently performed over a sequence of shorter intervals resulting in an approach referred to as *piecewise optimal*. The state reached by the optimized flow at the end of a given interval is taken as the starting point for optimization on the following interval. Of course, optimal controls determined separately on a sequence of intervals with length T *do not* combine into a globally optimal control on the whole optimization time-span. Certain general properties of the piecewise optimal control were studied by Heinkenschloss[30] who showed that the problem of computing piecewise optimal controls on adjacent intervals is related to the forward sweep of the Gauss–Seidel method for the solution of the related linear algebraic problem which has block structure. The piecewise optimal control approach to the 2D velocity tracking problem was addressed by Hou and Yan[31] who proved that the rate of the functional decrease is independent of the length T of the single optimization horizon. On the other hand, Bewley *et al.*[22] showed computational evidence that the effectiveness

of the control increases as the optimization horizon is extended until a certain value of T is reached beyond which it does not improve anymore. Further below we address these issues in the present problem.

III. "VORTICITY" FORM OF THE ADJOINT EQUATIONS

As discussed in the Introduction, we choose to solve the hydrodynamic equations (1) in the vorticity form (2). It is natural to apply the same solution method and the same solver to the adjoint equations formulated above. To this end it is necessary to derive the "vorticity" form of the system (9). We use the term "vorticity" in quotes, because this quantity is the curl of a field which is not, strictly speaking, the actual velocity field. Since this is a novel approach, we present it here first for the complete 3D system, and then specify the derivation to the 2D case. We take the curl of the first element in the expression corresponding to $N^*\boldsymbol{w}^*$ in (9) and immediately notice that the "pressure" term drops out and that the curl operator commutes with both the time derivative and the Laplacian. As regards the "advection" term, we have the following (here we have to use index notation for vector operations):

$$
\begin{aligned}
&[\nabla\times\{\boldsymbol{V}_0\cdot[\nabla\boldsymbol{w}^*+(\nabla\boldsymbol{w}^*)^T]\}]_m \\
&\quad=\varepsilon_{mkj}\frac{\partial}{\partial x_k}\left[V_{0i}\left(\frac{\partial w_j^*}{\partial x_i}+\frac{\partial w_i^*}{\partial x_j}\right)\right] \\
&\quad=\varepsilon_{mkj}\frac{\partial V_{0i}}{\partial x_k}\left(\frac{\partial w_j^*}{\partial x_i}+\frac{\partial w_i^*}{\partial x_j}\right) \\
&\qquad+\varepsilon_{mkj}V_{0i}\frac{\partial^2 w_j^*}{\partial x_i\partial x_k}+\varepsilon_{mkj}V_{0i}\frac{\partial^2 w_i^*}{\partial x_j\partial x_k} \\
&\quad=\underbrace{V_{0i}\frac{\partial}{\partial x_i}\varepsilon_{mkj}\frac{\partial w_j^*}{\partial x_k}}_{(\boldsymbol{V}_0\cdot\nabla)\boldsymbol{\omega}_A^*}+\underbrace{\varepsilon_{mkj}\frac{\partial V_{0i}}{\partial x_k}\left(\frac{\partial w_j^*}{\partial x_i}+\frac{\partial w_i^*}{\partial x_j}\right)}_{2\,\mathrm{dual}\{\nabla\boldsymbol{V}_0\cdot[\nabla\boldsymbol{w}^*+(\nabla\boldsymbol{w}^*)^T]\}}.
\end{aligned}
\tag{14}
$$

Here $\boldsymbol{\omega}_A^*=\nabla\times\boldsymbol{w}^*$ is the adjoint "vorticity," $[\circ]_m$ denotes the mth component of a given vector and ε_{mkj} is the Levi–Civita alternating tensor. The vector dual to a tensor is defined as $[\mathrm{dual}\mathbf{A}]_i=\frac{1}{2}\varepsilon_{ijk}A_{jk}$. In the above the term $\varepsilon_{mkj}V_{0i}(\partial^2 w_i^*/\partial x_j\partial x_k)$ vanishes due to symmetry of the tensor with the second derivatives of the quantity w_i^*. Consequently, the vorticity adjoint equation takes the form

$$
\begin{aligned}
&-\frac{\partial\boldsymbol{\omega}_A^*}{\partial t}-(\boldsymbol{V}_0\cdot\nabla)\boldsymbol{\omega}_A^*-\mu\Delta\boldsymbol{\omega}_A^* \\
&\qquad+2\,\mathrm{dual}\{\nabla\boldsymbol{V}_0\cdot[\nabla\boldsymbol{w}^*+(\nabla\boldsymbol{w}^*)^T]\}=0, \\
&\boldsymbol{\omega}_A^*=\nabla\times\boldsymbol{w}^*,\quad \nabla\cdot\boldsymbol{w}^*=0, \\
&\boldsymbol{w}^*=-\boldsymbol{g}\quad\text{on}\quad\Gamma_0,\quad \boldsymbol{w}^*\to 0\quad\text{for}\quad|x|\to\infty, \\
&\boldsymbol{w}^*|_{t=T}=0\quad\text{in}\quad\Omega.
\end{aligned}
\tag{15}
$$

The function $\boldsymbol{g}$ specifying the boundary condition is given in the Appendix [Eq. (A8)]. In the plane 2D case the above system reduces to ($\boldsymbol{\omega}_A^*=\omega_A^*\boldsymbol{e}_z$)

$$
\begin{aligned}
&-\frac{\partial\omega_A^*}{\partial t}-(\boldsymbol{V}_0\cdot\nabla)\omega_A^*-\mu\Delta\omega_A^*+2\left[\frac{\partial w_y^*}{\partial y}\left(\frac{\partial V_{0y}}{\partial x}+\frac{\partial V_{0x}}{\partial y}\right)\right. \\
&\qquad\left.+\frac{\partial V_{0x}}{\partial x}\left(\frac{\partial w_y^*}{\partial x}+\frac{\partial w_x^*}{\partial y}\right)\right]=0, \\
&\omega_A^*=\frac{\partial w_y^*}{\partial x}-\frac{\partial w_x^*}{\partial y},\qquad \frac{\partial w_x^*}{\partial x}+\frac{\partial w_y^*}{\partial y}=0, \\
&\boldsymbol{w}^*=-\boldsymbol{g}\quad\text{on}\quad\Gamma_0,\quad \boldsymbol{w}^*\to 0\quad\text{for}\quad|x|\to\infty, \\
&\boldsymbol{w}^*|_{t=T}=0\quad\text{in}\quad\Omega,
\end{aligned}
\tag{16}
$$

where $\boldsymbol{w}^*=[w_x^*,w_y^*,0]$. The source (i.e., the last) term in the 2D vorticity equation above can be expressed using components of the rate-of-strain tensors of the primal and the adjoint field as $s_{11}^0 s_{12}^*-s_{11}^* s_{12}^0$.

As was the case of the Navier–Stokes system, the adjoint "pressure" can be determined *a posteriori* from the Poisson equation obtained by taking the divergence of the momentum adjoint equation (9). After some elementary transformations this yields

$$
\begin{aligned}
&\Delta q^*=\nabla\boldsymbol{V}_0:[\nabla\boldsymbol{w}^*+(\nabla\boldsymbol{w}^*)^T]+\boldsymbol{V}_0\cdot\mu\Delta\boldsymbol{\omega}_A^*, \\
&(\boldsymbol{n}\cdot\nabla)q^*=\boldsymbol{n}\cdot\left\{-\frac{\partial\boldsymbol{w}^*}{\partial t}-\boldsymbol{V}_0\cdot[\nabla\boldsymbol{w}^*+(\nabla\boldsymbol{w}^*)^T]-\mu\Delta\boldsymbol{w}^*\right\}_\Gamma.
\end{aligned}
\tag{17}
$$

Similarly to the vorticity equation (2), in multiconnected domains systems (15) and (16) must be complemented with constraints on "vorticity" production on the boundary. They are obtained by projecting the momentum adjoint equation (9) on the direction $\boldsymbol{\tau}$ tangential to the boundary, integrating along the perimeter and requiring that there be no jump in pressure. In 2D this yields

$$
\begin{aligned}
\mu\oint_{\Gamma_0}\frac{\partial\omega_A^*}{\partial n}ds=&-\oint_{\Gamma_0}\left(\frac{\partial\boldsymbol{w}^*}{\partial t}\right)\cdot\boldsymbol{\tau}ds \\
&+\oint_{\Gamma_0}\left\{[(\boldsymbol{V}_0\cdot\nabla)\boldsymbol{w}^*]\cdot\boldsymbol{\tau}+\boldsymbol{w}^*\frac{\partial}{\partial s}\boldsymbol{V}_0\right\}ds.
\end{aligned}
\tag{18}
$$

This, together with (16) and (17), constitutes an equivalent formulation of the adjoint system (9) in 2D.

IV. NUMERICAL SIMULATIONS

All the simulations presented in this study are performed with the use of the Vortex Method. This is a Lagrangian approach to solving the 2D vorticity equation (2). The main idea consists in approximating the vorticity field using an unstructured superposition of vorticity particles with prescribed core functions. The system is advanced in time using viscous splitting which means that the advection and diffusion part of (2) are solved independently during one time step. Every particle, called the *vortex blob*, moves in the velocity field induced by all other particles and complemented with some potential contribution. Our Vortex Method uses the second-order accurate Gaussian core functions com-

bined with the second-order time splitting scheme. Exhaustive description of the implementation together with various benchmarks is presented in Refs. 9 and 32.

One of the novelties of this paper is the derivation and the solution of the ''vorticity'' form (16) of the adjoint system (9). Now we give some remarks concerning its solution using the Vortex Method. The system (16) constitutes a terminal value problem, however, using the substitution $t=T-\tau$ we obtain an initial value problem for the advection–diffusion equation with a source term. It can be marched forward in the time τ, i.e., backward in the ''physical'' time t. After this substitution, the adjoint system (16) is solved using essentially the same method as the primal system (2). The few modifications are addressed below. Advection in the adjoint system (16) takes place in the velocity field $\boldsymbol{V}_0$, i.e., the solution of the Navier–Stokes system around which the linearization is performed at a given iteration. However, as a result of the above substitution, the sign of the field $\boldsymbol{V}_0$ is reversed, and therefore, the adjoint flow develops in the direction opposite to the primal Navier–Stokes flow. The adjoint ''vorticity'' equation (16) differs from the vorticity equation (2) also in that it has the source term $Src=s_{11}^0 s_{12}^* + s_{11}^* s_{12}^0$. Apart from diffusion, this is the second mechanism which changes the strengths of the particles. The source term is evaluated at the centers of the particles and then the resulting circulation updates are computed. When the particle (i.e., Lagrangian) representation is used, the strain fields s_{11} and s_{12} have essentially the same localization as the vorticity field ω. This means that the source term Src practically vanishes away from the support of both the primal and the adjoint vorticity, and therefore, new circulation is not created there. Consequently, the source terms modifies the adjoint ''vorticity'' field via update of the strengths of the existing particles only. For comparable sizes, the computational cost of the adjoint problem is slightly larger than that of the primal. This is because the adjoint solver must handle two fields, i.e., the primal (in which advection takes place) and the dual, and must also account for the source term. Nevertheless, in practice the length of a single optimization horizon T is significantly shorter than the total time for which the flow is computed. Owing to the ever-expanding character of the Lagrangian mesh, the computational time per time step is proportional to the length of the interval over which we need to calculate the solution. Therefore, in our problem the support of the adjoint ''vorticity'' is much smaller than of the primal vorticity and, consequently, the size of the adjoint problem is usually much smaller than that of the primal. This is an advantage of using the ''vorticity'' form of the momentum adjoint equations.

V. RESULTS OF THE OPTIMAL CONTROL

In this section we present and analyze the results of the simulations using the optimal control algorithm. In all cases control is applied to the wake flow with developed vortex shedding. We briefly recall here that, in the spirit of the piecewise linear control, the whole optimization time-span is split into several intervals with the same length. Optimization is then performed on each of these and the flow state reached at the end of an interval is taken as the starting point for optimization on the following interval. Our investigations are performed at the Reynolds numbers of 75 and 150 which allows us to see how the algorithm handles flows characterized by different degrees of supercriticality. We also make an attempt at controlling the stationary flow at $Re=40$. This is intended to address the question whether the basic flow, i.e., the steady symmetric state, constitutes the limit of performance at a given Re. In Table I we summarize the numerical parameters (time step Δt, blob radius r_b and the approximate number of vortices N_b) used in the simulations of the flows at different Reynolds numbers. At a given Re, flows with different optimization horizons as well as the adjoint problem are computed with the same numerical parameters. Next, in Table II we summarize the parameters of the control in the different cases. Flows at $Re=40$, 75 and 150 are labeled A_α, B_α, and C_α, respectively, with the subscript α representing to the length of the optimization horizon. Hereafter these symbols will be used to refer to the particular controlled flows. In the table we give the lengths of the optimization horizons T and their ratios to the length of the natural vortex shedding period equal to 6.9 and 5.5 at $Re=75$ and $Re=150$, respectively. For the steady flow at $Re=40$ this quantity is obviously indeterminate. We also show the norms $\|\dot{\varphi}_{\mathrm{opt}}(t)\|_{L^2([0,T])}$ of the optimal controls which give an idea about their ''intensity.'' The control is switched on at the instant $t_0=100$ for $Re=40$, at $t_0=75$ for $Re=75$ and at $t_0=50$ for $Re=150$. Using the Vortex Method, the steady subcritical flow at $Re=40$ is computed as the limit correspond-

TABLE I. Numerical parameters used in the simulations at different Reynolds numbers Re. Time step is denoted Δt, blob radius r_b and approximate number of vortex blobs N_b.

Re	Δt	r_b	N_b ($\times 10^3$)
40	0.05	0.0278	150
75	0.05	0.0222	200
150	0.05	0.0178	300

TABLE II. Parameters of the control algorithm: T is the length of the optimization horizon and T/T_{VS} its ratio to the length of the natural vortex shedding period at a given Re, $\|\dot{\varphi}_{\mathrm{opt}}(t)\|_{L^2([0,T])}$ is the norm of the optimal control.

	Re	T	$\frac{T}{T_{\mathrm{VS}}}$	$\|\dot{\varphi}_{\mathrm{opt}}(t)\|_{L^2}$
A_4	40	4.0	⋯	0.030
A_5	40	5.0	⋯	0.012
A_6	40	6.0	⋯	0.040
B_1	75	1.0	0.15	0.032
B_2	75	2.0	0.29	0.040
B_3	75	3.0	0.44	0.041
B_4	75	4.0	0.58	0.042
B_5	75	5.0	0.73	0.039
B_6	75	6.0	0.87	0.041
C_1	150	1.0	0.18	0.069
C_2	150	2.0	0.36	0.089
C_3	150	3.0	0.54	0.076
C_4	150	4.0	0.72	0.141
C_5	150	5.0	0.91	0.114
C_6	150	6.0	1.08	0.123

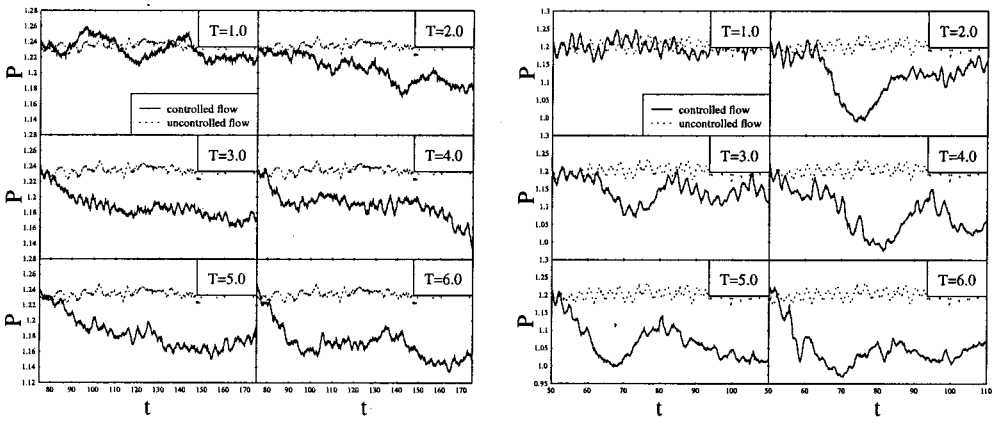

(a) Total power, $Re = 75$. (b) Total power, $Re = 150$.

FIG. 2. The total power P in the controlled flows with different optimization horizons and in the uncontrolled flows at $Re=75$ (a) and $Re=150$ (b).

ing to $t\to\infty$ of the unsteady flow instantaneously accelerated from rest. In such case at $t_0=100$ all the transients related to the instantaneous start are already sufficiently small. Convergence of the optimal control algorithm was usually achieved within 2 to 3 iterations. Every iteration required first solution of the Navier–Stokes system forward in time, then solution of the adjoint problem backward in time and finally a few (usually 5–7) evaluations of the functional, each of them involving solution of the Navier–Stokes system on the optimization interval. As explained above, the computational cost of the adjoint problem is usually slightly smaller than for the primal problem, nevertheless the overall cost of the optimization procedure is comparable to 12–20 solutions of the Navier–Stokes system on the optimization interval. Below we first proceed to discuss the control of the unsteady flows at $Re=75$ and $Re=150$ and then of the steady flow at $Re=40$.

The quantity which we in principle seek to minimize is the sum of the work done against the drag force and the work needed to control the flow. In Fig. 2 we present the temporal evolution of the total power $P=F_D\cdot|\boldsymbol{V}_\infty|+M\cdot\dot{\varphi}$ for flows at $Re=75$ and $Re=150$ with different optimization horizons and the flows with no control. We see that, apart from the cases with the shortest optimization horizons (B_1 and C_1), the total power is decreased for both values of Re. This confirms the effectiveness of the algorithm. Evidently, reduction is greater for longer optimization horizons. At $Re=75$ the total power is pushed down to a lower level around which it stabilizes. At $Re=150$ the total power oscillates around new values lower than in the uncontrolled flow. In Fig. 3 we present the time series of the control power P_C. We see that they are intermittent with occasional excursions to negative values. Spikes observed in Fig. 3 are related to sharp movements of the obstacle. In absolute terms, the reduction of the total power at $Re=75$ was smaller than at $Re=150$ by a factor of about two. So was the control power which at $Re=75$ was smaller than at $Re=150$ by a factor of about five.

Next in Fig. 4 we present the temporal evolution of the drag coefficient c_D, the quantity which is of greatest interest in most practical implementations. Its temporal behavior is in all cases very similar to the behavior of the total power P which is due to the very low lever of the control power P_C. In Fig. 4 we also indicate the drag values obtained in the

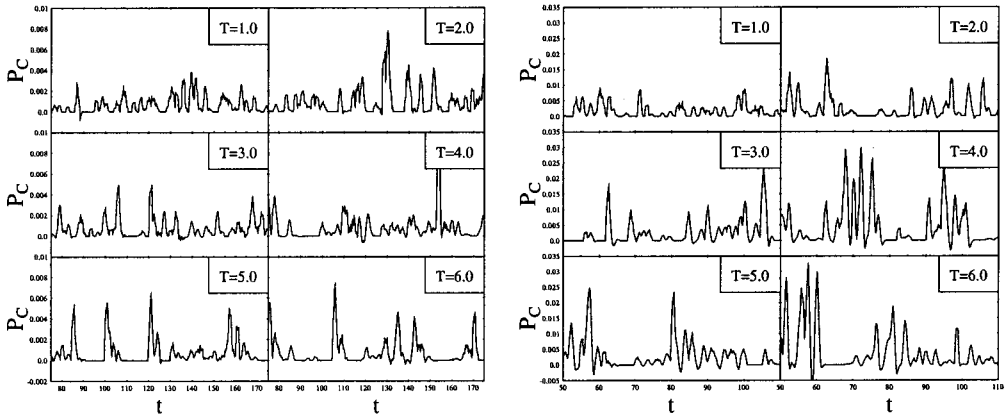

(a) Control power, $Re = 75$. (b) Control power, $Re = 150$.

FIG. 3. The control power P_C in the controlled flows with different optimization horizons at $Re=75$ (a) and $Re=150$ (b).

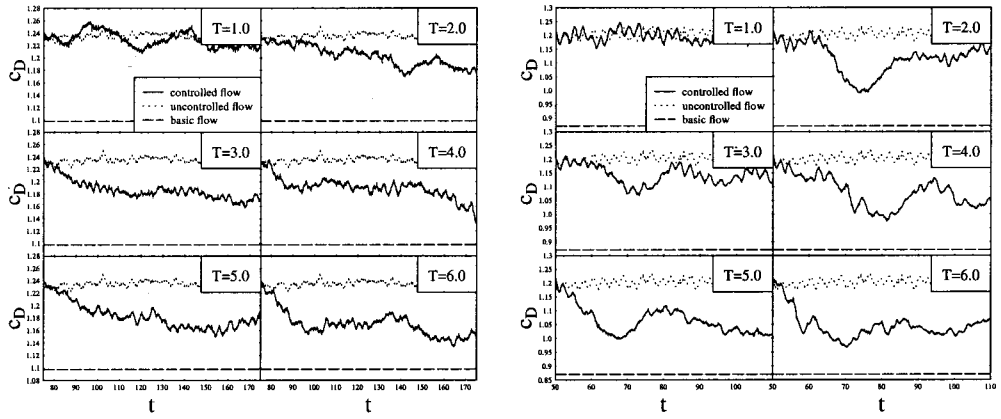

(a) Drag coefficient, $Re = 75$. (b) Drag coefficient, $Re = 150$.

FIG. 4. The drag coefficient c_D in the controlled flows with different optimization horizons and in the uncontrolled flows at $Re=75$ (a) and $Re=150$ (b). The values of drag in the basic flows are also indicated.

unstable, steady, symmetric states (i.e., the *basic flows*) at the same Re. In the flow at $Re=75$ with the longest optimization horizon $T=6.0$ the drag is driven down to about 93% of its value in the uncontrolled flow. For $Re=150$ and $T=6.0$ drag oscillates at about 85% of its original value.

For both values of Re the amount of the sustained drag decrease grows as the optimization horizon is extended and reaches maximum at values of T comparable to the length of the vortex shedding period. As the results for the cases C_4, C_5, and C_6 show, longer optimization horizons primarily reduce the amplitude of oscillations around the new values of the mean drag. Our additional investigations (not reported here) indicate that extension of the optimization horizon beyond the natural vortex shedding period does not improve effectiveness of the control anymore. Similar behavior of the optimal control algorithm with respect to the length of the optimization horizon was observed by Bewley *et al.* in Ref. 22 for the case of the turbulent channel flow. We propose the following simple rationale to explain this behavior—for intermediate values of T, i.e., smaller than some characteristic time scale of the phenomenon (the natural vortex shedding period in the present study), the effectiveness of the algorithm increases as we extend T and thereby look farther ahead while optimizing the flow. However, when the characteristic time scale of vortex shedding is reached, further extension of the optimization horizon T does not bring in significantly new information, and therefore, the algorithm does not perform any better. We note that this second regime is consistent with the theoretical predictions of Hou and Yan[31] mentioned earlier in Sec. II.

As shown by Protas and Wesfreid in Ref. 9, in the supercritical wake flow the mean drag consists of the two contributions: The drag of the *basic flow* (i.e., the unstable, steady, symmetric solution) which at a given Re remains fixed and the drag of the *mean flow correction* which is due to the presence of the vortex shedding and can be affected by a suitable modification of how the vortices are created and shed. As the Reynolds number increases, the relative contribution of the oscillatory part of the flow to drag becomes more significant. In Fig. 4 we marked the values of drag in the corresponding basic flows, so that the intervals above them indicate the drag related to the Bénard–von Kármán vortices. We note that at $Re=75$ and for $T=6.0$ the control is able to annihilate about 62% of the drag related to vortex

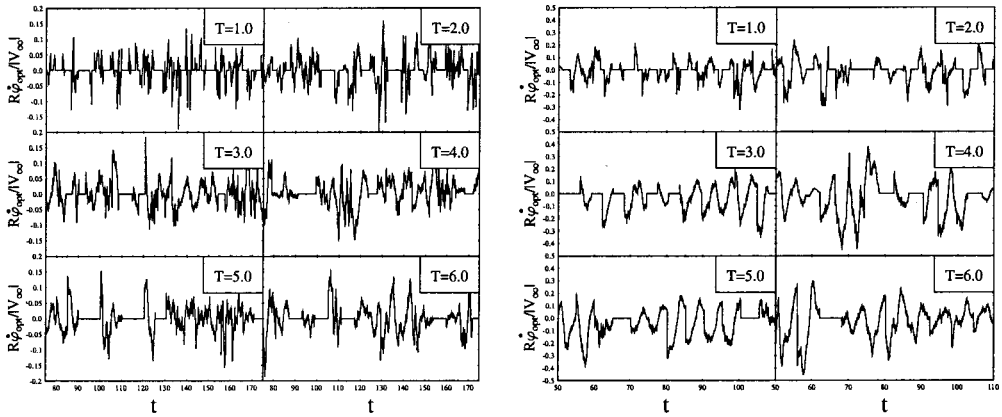

(a) Optimal controls, $Re = 75$. (b) Optimal controls, $Re = 150$.

FIG. 5. The optimal controls $\dot{\varphi}_{\mathrm{opt}}(t)$ determined by the algorithm for the flows at $Re=75$ (a) and $Re=150$ (b).

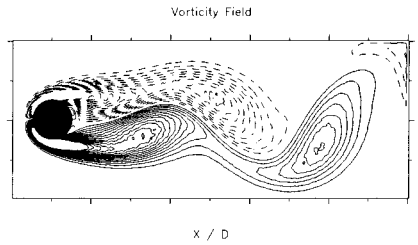

(a) no control

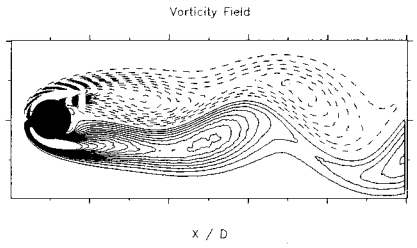

(b) $t = 105$

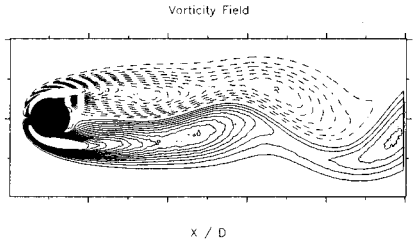

(c) $t = 147$

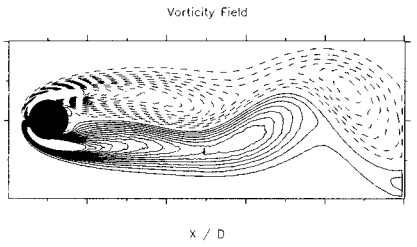

(d) $t = 177$

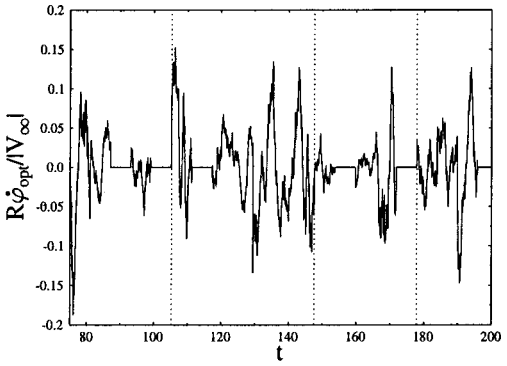

(e) Optimal control, $Re = 75$, $T = 6.0$

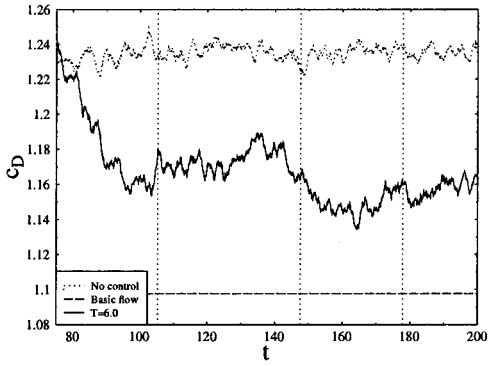

(f) Drag coefficient, $Re = 75$, $T = 6.0$

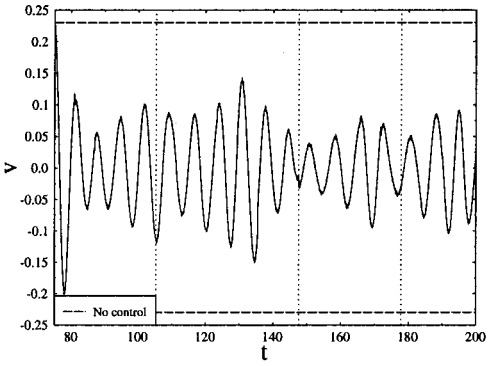

(g) transverse velocity at $(1.5, 0.0)$, $Re = 75$, $T = 6.0$

FIG. 6. Snapshots of the vorticity fields corresponding to the uncontrolled flow (a) and the distinctive stages of the optimization process (b)–(d), and the traces of the optimal control $\dot{\varphi}_{\text{opt}}(t)$ (e), the drag coefficient c_D (f) and the transverse velocity v at the point (1.5,0.0) (g) for $Re=75$ and $T=6.0$. Except for the top figure, the vorticity fields correspond to the instances of time marked by the vertical lines in the figures on the right. For clarity, the contour lines for the extremal vorticity values are not shown in the vorticity plots.

shedding and about 54% at $Re=150$. Thus, at a lower Re the control manages to suppress a larger fraction of the drag due to the oscillatory part of the flow. The reason for this is that the instability can be more easily controlled at a lower Re. Further below we address this issue in terms of the flow patterns.

Now in Fig. 5 we characterize the optimal controls, the rotation rates $\dot{\varphi}_{\text{opt}}(t)$, that were determined by the algorithm. The plots are normalized and give the circumferential velocity of the obstacle in units of the free stream. The first observation is that the magnitude of control is indeed rather small, with the circumferential velocity of the obstacle being on the order of 2%–5% for $Re=75$ and 10%–20% for $Re=150$ of the free stream (see also the quantity $\|\dot{\varphi}_{\text{opt}}(t)\|_{L^2([0,T])}$ in Table II). The optimized controls are characterized by the presence of step-like discontinuities at

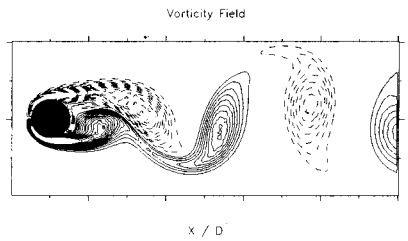

(a) no control

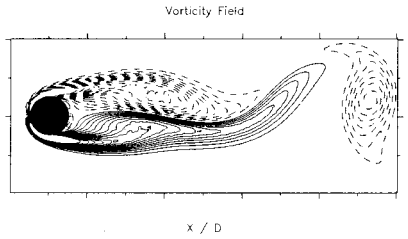

(b) $t = 68$

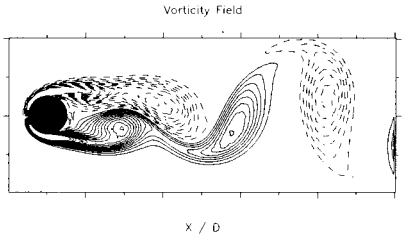

(c) $t = 80$

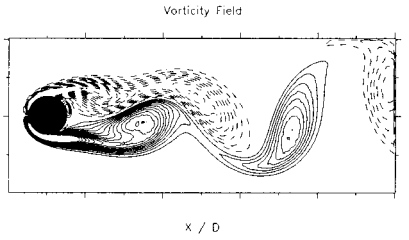

(d) $t = 104$

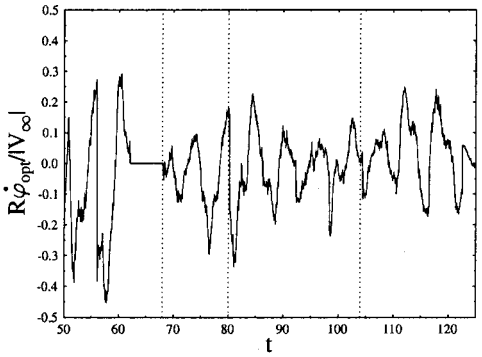

(e) Optimal control, $Re = 150$, $T = 6.0$

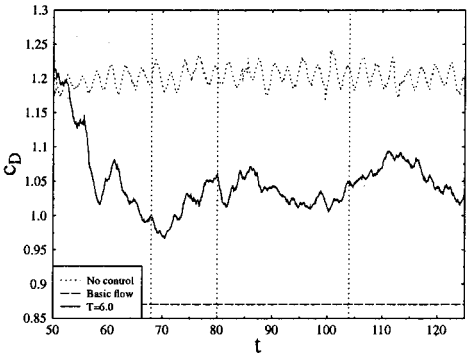

(f) Drag coefficient, $Re = 150$, $T = 6.0$

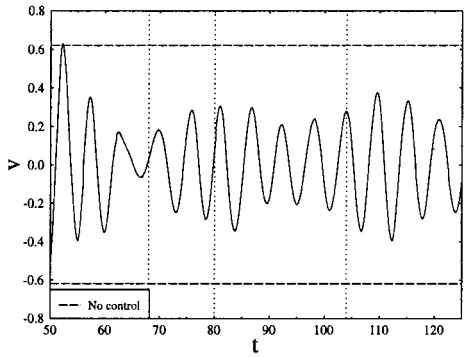

(g) transverse velocity at $(1.5, 0.0)$, $Re = 150$, $T = 6.0$

FIG. 7. Snapshots of the vorticity fields corresponding to the uncontrolled flow (a) and the distinctive stages of the optimization process (b)–(d), and the traces of the optimal control $\dot{\varphi}_{opt}(t)$ (e), the drag coefficient c_D (f) and the transverse velocity v at the point (1.5,0.0) (g) for $Re=150$ and $T=6.0$. Except for the top figure, the vorticity fields correspond to the instances of time marked by the vertical lines in the figures on the right. For clarity, the contour lines for the extremal vorticity values are not shown in the vorticity plots.

the boundaries between two optimization intervals. The controls on adjoining intervals are determined independently and there is no mechanism assuring that they should be continuous across the boundary. These issues are more systematically investigated by Heinkenschloss.[30] At the same time, discontinuity of the rotation rate does not cause difficulties in the solution of the problem. In Fig. 5 we also see that there are intervals with zero control interwoven with intervals where the control does not vanish. As already pointed out in Sec. II, the zero control is an adjustment related to approximate line minimization of the functional in the case when the optimal value of α_i in (11) turns out to be significantly smaller than the range of α's tested during the given line minimization. This set of α's depends on the initial guess which is fixed during the simulation with a given optimization horizon and it may occasionally happen that for certain intervals this initial guess may fall outside the validity range of the Gâteaux differential (i.e., the linear approximation). In such case it might be difficult to find within the allowed number of flow evaluations (usually 4 to 5) a value of α

resulting in a sufficient decrease of the functional. Nevertheless, this can only happen when the functional gradient has a relatively small magnitude and allowing for a few more flow evaluations would make it possible to find a nonzero control. However, the amplitude of this solution would be very small, as it would correspond to values of α_i much smaller than the ones determined on other intervals. Consequently, the decrease of the functional comparing to its value obtained for the zero control would also be very small (proportional to the small optimal α_i). At the same time, the computational cost of this more accurate line minimization would be significantly increased. Therefore, for practical reasons, we leave the zero control in cases when no functional decreasing solution is found within the number of allowed functional evaluations. Given these observations, the presented results are in fact to be regarded as approximations of the optimal controls obtained with the numerical accuracy that we could afford. All the controls shown in Fig. 5 appear fairly spiky and irregular, nevertheless, for the cases C_3-C_6 some long time regularity can be traced in the time series. In fact, the tendency of the optimal control algorithm to develop spiky controls was also evidenced in other related studies, namely, by Graham *et al.*[14] and He *et al.*[7]

Based on the obtained optimal controls, we made an attempt at extracting simple open-loop controls hoping to reproduce the drag reduction. The extraction was done in the simplest possible fashion—the actual control for the cases B_4, B_5, B_6 and C_4, C_5, C_6 was replaced with a harmonic oscillation at the frequency and amplitude approximately determined from Fig. 5 (phase information was not taken into account). Thus designed open-loop controller failed to achieve drag reduction. Conversely, drag was increased even above the uncontrolled level indicating that preserving the fine structure of the optimal control is essential for successfully extracting open-loop controls. This finding has practical implications, as it shows that the derived open-loop controller must retain some small-scale features of the optimal controls.

We recapitulate this part by analyzing the correlation between the optimal control $\dot{\varphi}_{\mathrm{opt}}(t)$, modifications of the drag and changes in the flow pattern. In Fig. 6 we present evolutions of the optimal control $\dot{\varphi}_{\mathrm{opt}}(t)$, the drag coefficient c_D and the transverse velocity v on the centerline for the control with the optimization horizon $T=6.0$ and the Reynolds number $Re=75$ (case B_6). In the figure we also show snapshots of the vorticity fields at the instances corresponding to the distinctive stages of the flow pattern development. On the temporal plots these instances are marked by vertical dashed lines. In Fig. 7 we present analogous data for $Re=150$ and $T=6.0$ (case C_6). First we discuss the results for the case B_6. When the control is switched on, drag rapidly drops to some intermediate value and after some time drops to a still lower value around which it stabilizes. The snapshots of the vorticity field correspond to the beginning of the intermediate plateau, the middle of the following drop and an intermediate point during the final stabilization. In all the figures we see that control acts to suppress the vortex shedding and the resulting flow approaches the symmetric state with elongated recirculation bubble. As regards the optimal control $\dot{\varphi}_{\mathrm{opt}}(t)$, intervals of the strongest activity coincide with the intermediate stage corresponding to the plateau. In the case C_6, when the control is switched on, the drag first also abruptly drops, and then oscillates about the new mean value. In both cases we see that the optimal control results in a significant reduction of the transverse velocity oscillations comparing to the uncontrolled flow and that the largest reduction is correlated with the sharpest decrease of drag. The plots of the transverse velocity also give an idea about the number of the vortex shedding cycles covered in the simulation.

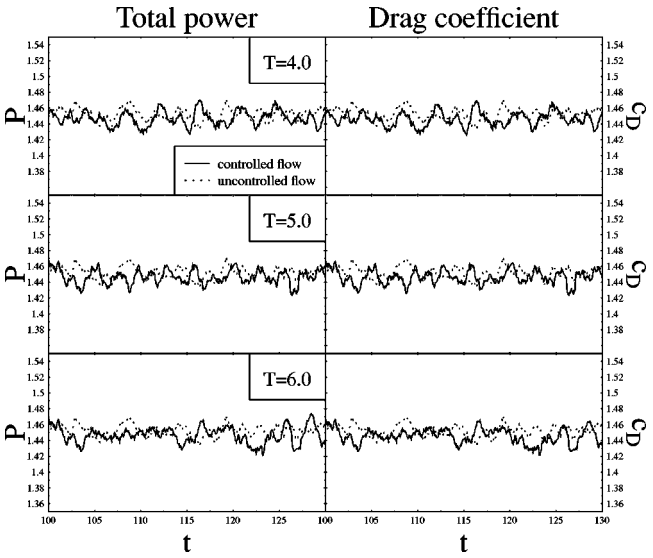

FIG. 8. Time history of the total power P (left) and the drag coefficient c_D (right) for the controlled flows with different optimization horizons and the uncontrolled flow at $Re=40$.

Our presentation of the results is concluded by showing the data for the subcritical case with $Re=40$. In Fig. 8 we show the total power P and the drag coefficient c_D obtained in the controlled flows with three optimization horizons $T=4.0$, 5.0, and 6.0 (cases A_4, A_5, and A_6). We see that no reduction of either the total power P or the drag c_D has been achieved in any of the three cases.

Finally, we present samples of the adjoint ''vorticity'' fields. This is intended to give an idea of what the adjoint field looks like and how its evolution compares to that of the primal flow. In Fig. 9 we present snapshots of the primal vorticity (right column) and of the corresponding adjoint ''vorticity.'' By primal vorticity we mean the curl of the velocity field obtained from the forward in time integration of the Navier–Stokes system, whereas the adjoint ''vorticity'' is the solution of the backward in time adjoint system in the form (16). In the figure we show the fields obtained in the case C_6 during the first iteration over the optimization interval [50;56]. We show snapshots taken at the instances of time $t=50.5$ (top), 53.0 (middle) and 55.5 (bottom) which correspond, respectively, to the beginning, the middle and the end of the optimization interval. Note that, as discussed in Sec. II, the adjoint field vanishes at the end of the optimization interval (bottom figures), and develops backward in time. When viewed from the bottom to the top, the adjoint field

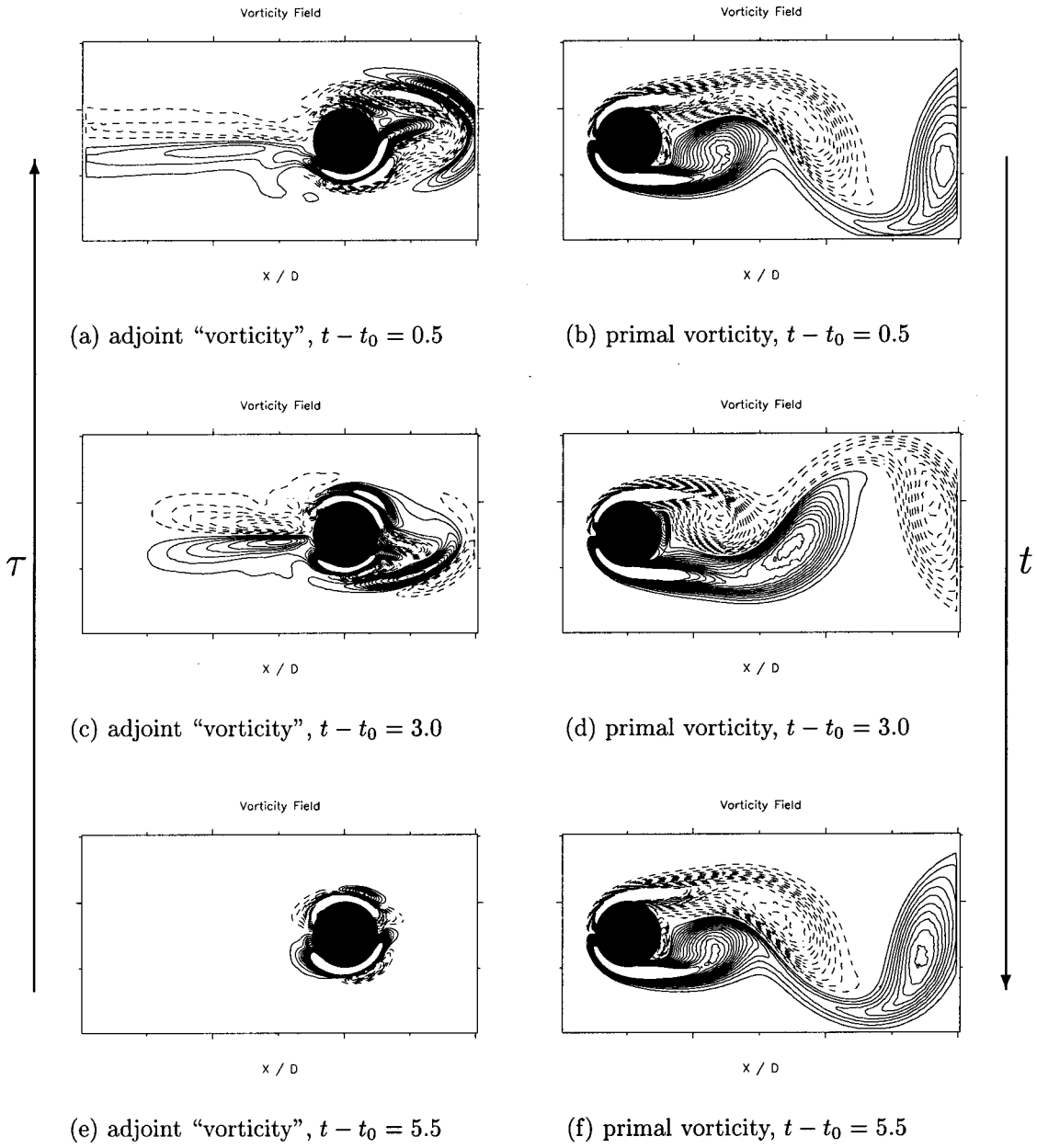

FIG. 9. Fields of the adjoint (left) and the primal (right) vorticity at the different stages during one optimization interval for the case C_6. The fields shown here correspond to the first iteration over the interval [50, 56] ($t-t_0$ denotes the time elapsed since the control was switched on). For clarity, the contour lines for the extremal vorticity values are not shown. Arrows indicate the directions of the primal and the adjoint times, t and τ, respectively.

grows upstream, i.e., in the direction opposite to the primal field (this is due to the reversed sign of the field $\boldsymbol{V}_0$ in (16) resulting from the substitution $t=T-\tau$). The physical meaning the adjoint field is that the integral (10), involving boundary values of strain associated with this field, represents the sensitivity of the functional (5) to the particular kind of forcing.

VI. CONCLUSIONS

The presented results indicate that the algorithm does indeed decrease drag, provided the optimization horizon is sufficiently long. The maximum sustained drag reduction is obtained when the optimization horizon becomes comparable to the length of the natural vortex shedding period, which may suggest that optimization could practically be reduced to controlling a single shedding event. The drag reduction in the best cases was 7% at $Re=75$ and 15% at $Re=150$. Even though the presented algorithm is formally optimal, in the actual numerical calculations we can only compute an approximation of the optimal control. This approximation becomes more accurate when numerical parameters are refined. We believe that our results could still be marginally improved by increasing the accuracy of line minimizations. This would, however, greatly increase the computational cost which is already large, and therefore, would not allow us to examine that many configurations. We note that in a related study using similar methods He *et al.*[7] obtained about 3% improvement over the control based on sinusoidal

rotation at $Re=200$. It is remarkable that in the present study the average level of the control power was very small, smaller by more than one order of magnitude than the gain in the total power. The energetic efficiency of the algorithm can be quantified by examining the *Power Saving Ratio* (PSR) defined as

$$\mathrm{PSR}=\frac{\Delta P_D}{P_C}. \tag{19}$$

The values of PSR obtained in the cases B_6 and C_6 are, respectively, 122 and 51. The efficiency of the present algorithm is thus significantly higher than in the suboptimal control approach developed by Min and Choi in Ref. 24 where the PSR did not exceed 2 or 3, even though in that case the net drag reduction was higher. This is evidence for the ''subtleness'' of the method developed here. We notice, however, that efficiency of the algorithm as represented by PSR deteriorates as the Reynolds number increases. This is also related to the increase of the amplitude of the optimal rotation rate (approximately by the factor of four as the Reynolds number is doubled). In the case of a circular obstacle the rotary control solely exploits viscous effects and their relative control authority decreases for higher Re when nonlinear inertial effects obviously become more important. One may thus conjecture that the control efficiency should be somehow inversely proportional to the intensity of vortex shedding. The Landau model (see, e.g., Mathis *et al.*[33]) characterizes this intensity using the transverse velocity v on the centerline whose amplitude scales as $(Re-Re_c)^{1/2}$, where $Re_c\approx 46$ marks the onset of vortex shedding. Indeed, we observe that the heuristic relation $\mathrm{PSR}(Re)\sim(Re-Re_c)^{-1/2}$ is approximately verified by the PSR values at the two investigated Reynolds numbers. Lower efficiency of the algorithm may thus explain the increase of the optimal rotation amplitude with Re. On the other hand, the present algorithm attempts to find the optimal control and from the study by He *et al.*[7] it is known that the ''optimal'' amplitude for the harmonic rotary control lies in a still higher range.

It follows from the above estimate that at much higher Re the efficiency of the algorithm could further drop. This, together with its large computational cost (requiring solution of the Navier–Stokes and the adjoint system several times over the optimization interval) makes the algorithm rather inapplicable under practical conditions. However, the goal of the present investigation was to use the Optimal Control approach to assess the fundamental capabilities and limitations of the rotary control of the unsteady wake. Optimal controls could be used to extract open–loop control laws, but more sophisticated reduction techniques are required. Our optimal control algorithm failed to achieve any success in controlling the subcritical flow at $Re=40$. This seems to support the conjecture that the steady symmetric flow represents the lower bound on the performance of this control configuration in terms of the functional (5).

The control configuration investigated in this study consists of just a single degree of freedom at every instant of time. This could explain why our optimization procedure required less iterations than in the study by Bewley *et al.*,[22] where the dimension of the control was much higher. On the other hand, this can also be the reason why the rotary control may be less effective than distributed blowing and suction. In the latter case the control dimension is much higher and the control possesses more authority over the flow.

One of the novelties of this paper consists in the derivation and the solution of the ''vorticity'' form (16) of the adjoint problem (9). When one is using the Vortex Method, this approach leads to important advantages. Finally, we wish to say a few words about further perspectives. Perhaps a better performance could be achieved by using a different functional not directly linked to drag. It was shown that formulations based on the functional targeting the terminal kinetic energy (Bewley *et al.* in Ref. 22) or the departure from some target flow (e.g., Min and Choi in Ref. 24) performed better than those directly targeting drag. In our case, given the relation between vortex shedding and drag, penalizing the departure from the steady, symmetric basic flow could be an alternative. Furthermore, as shown by Collis *et al.*,[34] the use of a carefully chosen Hilbert space to extract the gradient can enhance the regularity of the control. Another innovation would be to consider control of the flow past a noncircular obstacle. In this case the control would involve not only the wall-tangential, but also the wall-normal velocity component.

ACKNOWLEDGMENTS

The authors acknowledge the financial support of the Polish State Committee for Scientific Research (Grant No. KBN 7 T07A 007 16) and the program POLONIUM (Grant No. 99158). Parts of the computations were performed at ICM UW and PJWSTK. The authors have benefited from the discussions with J. Rokicki and J. Szumbarski. Shankar Subramaniam kindly provided the authors with a part of his vortex code.

APPENDIX: DERIVATION OF THE ADJOINT SYSTEM

As was shown by Abergel and Temam in Ref. 18, the quantities $\{\boldsymbol{w}(h);q(h)\}$ appearing in the Gâteaux differential (7) are related to the Fréchet differential of the mapping $\dot{\varphi}\rightarrow\{\boldsymbol{V}(\dot{\varphi});p(\dot{\varphi})\}$ and thus can be obtained as the solution of the Navier–Stokes system linearized about the state $\{\boldsymbol{V}_0(\dot{\varphi});p_0(\dot{\varphi})\}$

$$N\begin{bmatrix}\boldsymbol{w}\\ q\end{bmatrix}=\begin{bmatrix}\dfrac{\partial \boldsymbol{w}}{\partial t}+(\boldsymbol{V}_0\cdot\nabla)\boldsymbol{w}+(\boldsymbol{w}\cdot\nabla)\boldsymbol{V}_0-\mu\Delta\boldsymbol{w}+\nabla q\\ -\nabla\cdot\boldsymbol{w}\end{bmatrix}=\begin{bmatrix}0\\ 0\end{bmatrix},$$

$$\boldsymbol{w}|_{t=0}=0 \quad \text{in} \quad \Omega, \tag{A1}$$

$$\boldsymbol{w}=h\boldsymbol{\tau} \quad \text{on} \quad \Gamma_0, \quad \boldsymbol{w}\rightarrow 0 \quad \text{for} \quad |x|\rightarrow\infty.$$

The control perturbation h does not explicitly appear in the Gâteaux differential (7), as it enters only through solutions of (A1). In order to factor it out we will employ the *adjoint operator* N^* and the *adjoint state* $\{\boldsymbol{w}^*;q^*\}$ defined by the following relation:

$$\left(N\begin{bmatrix}\boldsymbol{w}\\ q\end{bmatrix},\begin{bmatrix}\boldsymbol{w}^*\\ q^*\end{bmatrix}\right)_{L^2(0,T;L^2(\Omega))}=\left(\begin{bmatrix}\boldsymbol{w}\\ q\end{bmatrix},N^*\begin{bmatrix}\boldsymbol{w}^*\\ q^*\end{bmatrix}\right)_{L^2(0,T;L^2(\Omega))}+B. \tag{A2}$$

Note that since N and N^* are ''two-element'' operators, the scalar products in (A2) are in fact defined on Cartesian products of two spaces $L^2(0,T;L^2(\Omega))$

$$\left(\begin{bmatrix}a\\ b\end{bmatrix},\begin{bmatrix}c\\ d\end{bmatrix}\right)_{L^2(0,T;L^2(\Omega))}=(a,c)_{L^2(0,T;L^2(\Omega))}+(b,d)_{L^2(0,T;L^2(\Omega))}. \tag{A3}$$

In (A2) B stands for the sum of the boundary terms obtained using integration by parts and the divergence theorem

$$\begin{aligned}B=&-\int_0^T\oint_{\Gamma_0}[(\boldsymbol{V}_0\boldsymbol{w})+(\boldsymbol{V}_0\boldsymbol{w})^T]:(\boldsymbol{w}^*\boldsymbol{n})d\sigma dt\\&-\mu\int_0^T\oint_{\Gamma_0}\{\boldsymbol{w}^*\cdot[\nabla\boldsymbol{w}+(\nabla\boldsymbol{w})^T]\\&-\boldsymbol{w}\cdot[\nabla\boldsymbol{w}^*+(\nabla\boldsymbol{w}^*)^T]\}\boldsymbol{n}d\sigma dt\\&-\int_0^T\oint_{\Gamma_0}(q\boldsymbol{w}^*-q^*\boldsymbol{w})\cdot\boldsymbol{n}d\sigma dt\\&+\left[\int_\Omega\boldsymbol{w}\cdot\boldsymbol{w}^*d\Omega\right]_{t=0}^{t=T}.\end{aligned} \tag{A4}$$

The symbol '':'' denotes contraction of two tensors ($\bar{\bar{A}}:\bar{\bar{B}}=A_{ij}B_{ij}$) and ***(ab)*** is the dyadic product of the vectors $\boldsymbol{a}$ and $\boldsymbol{b}$ [i.e., the tensor $(\boldsymbol{ab})_{ij}=a_ib_j$]. The adjoint state $\{\boldsymbol{w}^*;q^*\}$ is the solution of the problem *adjoint* to the linearized Navier–Stokes system (A1)

$$\begin{aligned}N^*\begin{bmatrix}\boldsymbol{w}^*\\ q^*\end{bmatrix}&=\begin{bmatrix}-\dfrac{\partial\boldsymbol{w}^*}{\partial t}-\boldsymbol{V}_0\cdot[\nabla\boldsymbol{w}^*+(\nabla\boldsymbol{w}^*)^T]-\mu\Delta\boldsymbol{w}^*+\nabla q^*\\ -\nabla\cdot\boldsymbol{w}^*\end{bmatrix}\\&=\begin{bmatrix}0\\ 0\end{bmatrix},\end{aligned}$$

$$\boldsymbol{w}^*|_{t=T}=0 \quad \text{in} \quad \Omega, \tag{A5}$$

$$\boldsymbol{w}^*=-\boldsymbol{g} \quad \text{on} \quad \Gamma_0, \quad \boldsymbol{w}^*\to 0 \quad \text{for} \quad |x|\to\infty.$$

In the case of the rotating circular cylinder the control is limited to the tangential boundary velocity. This implies that

$$(\boldsymbol{V}_0\cdot\boldsymbol{n})|_{\Gamma_0}=0, \tag{A6}$$

$$(\boldsymbol{w}\cdot\boldsymbol{n})|_{\Gamma_0}=0, \tag{A7}$$

and the integrals in (A4) which involve these terms vanish. Now the crucial issue is the determination of the boundary condition for the adjoint state $\boldsymbol{w}^*$, i.e., the function $\boldsymbol{g}$ in (A5). Our choice is motivated by the observation that, if $\boldsymbol{g}$ is judiciously matched, then in expression (A4) there appear terms identical to the ones present in the first part of (7). It is straightforward to verify that for the particular choice

$$\boldsymbol{g}=V_\tau\boldsymbol{\tau}+\boldsymbol{V}_\infty=\boldsymbol{r}\times(\dot{\varphi}\boldsymbol{e}_z)+\boldsymbol{V}_\infty, \tag{A8}$$

the boundary terms present in (A4) can be used to re-express the Gâteaux differential (7) in such a way that the control perturbation h explicitly appears in all the terms. In this way we obtain (8).

[1] R. Mittal and S. Balachandar, ''Effect of three-dimensionality on the lift and drag of nominally two-dimensional cylinders,'' Phys. Fluids **7**, 1841 (1995).
[2] R. D. Henderson, ''Details of the drag curve near the onset of vortex shedding,'' Phys. Fluids **7**, 2102 (1995).
[3] C. H. K. Williamson, ''Vortex dynamics in the wake,'' Annu. Rev. Fluid Mech. **28**, 477 (1996).
[4] P. Tokumaru and P. Dimotakis, ''Rotary oscillation control of a cylinder wake,'' J. Fluid Mech. **224**, 71 (1991).
[5] D. Shiels, ''Simulation of controlled bluff body flow with a viscous vortex method,'' Ph.D. thesis, California Institute of Technology (1998).
[6] X.-Y. Lu and J. Sato, ''A numerical study of flow past a rotationally oscillating circular cylinder,'' J. Fluids Struct. **10**, 829 (1996).
[7] J. W. He, R. Glowinski, R. Metcalfe, A. Nordlander, and J. Periaux, ''Active control and drag optimization for flow past circular cylinder,'' J. Comput. Phys. **163**, 83 (2000).
[8] C. Homescu, I. M. Navon, and Z. Li, ''Suppression of vortex shedding for flow around circular cylinder using optimal control,'' Int. J. Numer. Methods **38**, 43 (2002).
[9] B. Protas and J.-E. Wesfreid, ''Drag force in the open-loop control of the cylinder wake in the laminar regime,'' Phys. Fluids **14**, 810 (2002).
[10] M. D. Gunzburger and H. C. Lee, ''Feedback control of Kármán vortex shedding,'' Trans. ASME, J. Appl. Mech. **63**, 828 (1996).
[11] D. S. Park, ''Theoretical analysis of feedback control of Kármán vortex shedding at slightly supercritical Reynolds numbers,'' Eur. J. Mech. B/Fluids **13**, 387 (1994).
[12] K. Roussopoulos, ''Feedback control of vortex shedding at low Reynolds numbers,'' J. Fluid Mech. **248**, 267 (1993).
[13] W. R. Graham, J. Peraire, and K. Y. Tang, ''Optimal control of vortex shedding using low-order models. Part I—Open-loop model development,'' Int. J. Numer. Methods Eng. **44**, 945 (1999).
[14] W. R. Graham, J. Peraire, and K. Y. Tang, ''Optimal control of vortex shedding using low-order models. Part II—Model-based control,'' Int. J. Numer. Methods Eng. **44**, 973 (1999).
[15] S. I. Chernyshenko, ''Stabilization of trapped vortices by alternating blowing and suction,'' Phys. Fluids **7**, 802 (1995).
[16] L. Cortelezzi, ''Nonlinear feedback control of the wake past a plate with a suction point on the downstream wall,'' J. Fluid Mech. **327**, 303 (1996).
[17] L. Cortelezzi, Y.-C. Chen, and H.-L. Chang, ''Nonlinear feedback control of the wake past a plate: From a low order model to a higher order model,'' Phys. Fluids **9**, 2009 (1997).
[18] F. Abergel and R. Temam, ''On some control problems in fluid mechanics,'' Theor. Comput. Fluid Dyn. **1**, 303 (1990).
[19] J.-L. Lions, *Contrôle Optimal des Systèmes Gouverné par des Equations aux Dérivées Partialles* (Dunod, Paris, 1969) (English translation, Springer-Verlag, New York, 1971).
[20] H. Choi, R. Temam, P. Moin, and J. Kim, ''Feedback control for unsteady flow and its application to the stochastic Burgers equation,'' J. Fluid Mech. **253**, 509 (1993).
[21] Ch. Lee, J. Kim, and H. Choi, ''Suboptimal control of turbulent channel flow for drag reduction,'' J. Fluid Mech. **358**, 245 (1998).
[22] T. R. Bewley, P. Moin, and R. Temam, ''DNS-based predictive control of turbulence: an optimal benchmark for feedback algorithms,'' J. Fluid Mech. **447**, 179 (2001).
[23] S. S. Sritharan, ''An optimal control problem in exterior hydrodynamics,'' Proc. R. Soc. Edinburgh, Sect. A: Math. **121**, 5 (1992).
[24] Ch. Min and H. Choi, ''Suboptimal feedback control of vortex shedding at low Reynolds numbers,'' J. Fluid Mech. **401**, 123 (1999).
[25] M. D. Gunzburger and J. S. Peterson, ''Finite-element methods for the streamfunction-vorticity equations: Boundary-condition treatments and

multiply connected domains,'' SIAM (Soc. Ind. Appl. Math.) J. Sci. Stat. Comput. **9**, 650 (1988).
[26]T. R. Bewley, R. Temam, and M. Ziane, ''A general framework for robust control in fluid mechanics,'' Physica D **138**, 360 (2000).
[27]A. V. Fursikov, M. D. Gunzburger, and L. S. Hou, ''Boundary value problems and optimal boundary control for the Navier–Stokes system: The two–dimensional case,'' SIAM J. Control Optim. **36**, 852 (1998).
[28]E. Polak, *Computational Methods in Optimization* (Academic, New York, 1971).
[29]W. H. Press, B. P. Flanner, S. A. Teukolsky, and W. T. Vetterling, *Numerical Recipes: The Art of Scientific Computations* (Cambridge University Press, Cambridge, 1986).
[30]M. Heinkenschloss, ''Time-domain decomposition iterative methods for the solution of distributed linear quadratic optimal control problems,'' CAAM Technical Report TR00-31, Rice University, Houston, TX (2000).
[31]L. S. Hou and Y. Yan, ''Dynamics and approximations of a velocity tracking problem for the Navier–Stokes flows with piecewise distributed controls,'' SIAM J. Control Optim. **35**, 1847 (1997).
[32]B. Protas, ''Analysis and control of aerodynamic forces in the plane flow past a moving obstacle—Application of the vortex method,'' Ph.D. thesis, Warsaw University of Technology and Université Pierre et Marie Curie, (2000).
[33]C. Mathis, M. Provansal, and L. Boyer, ''The Bénard–von Kármán instability: Transient and forced regimes,'' J. Fluid Mech. **182**, 1 (1987).
[34]S. S. Collis, K. Ghayour, M. Heinkenschloss, M. Ulbrich, and S. Ulbrich, ''Towards adjoint-based methods for aeroacoustic control,'' AIAA Pap. 2001-0821 (2001).